





pubs.acs.org/crystal

# Anhydrous vs Hydrated f-Element Acetate Polymers Dictated by the Stoichiometry of Protic Acidic/Basic Azole Mixtures

Amrita Nayak, Volodymyr Smetana, Anja-Verena Mudring,\* and Robin D. Rogers\*



Cite This: Cryst. Growth Des. 2021, 21, 2516-2525



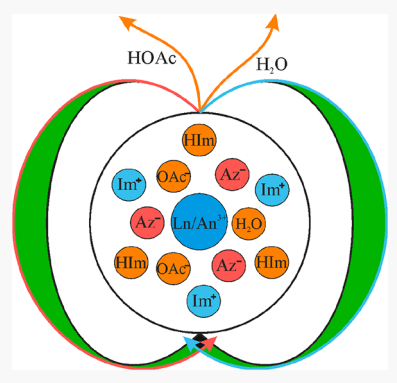
**ACCESS** 

Metrics & More

Article Recommendations

s Supporting Information

**ABSTRACT:** Continuing our investigations of ionic liquid (IL) based routes to a library of f-element/soft donor complexes which could be studied crystallographically, we have explored the dissolution of f-element salts in protic imidazole-based ILs containing only soft donors at high temperatures to drive off volatiles, including water and carboxylic or mineral acids. Here we present our results, reacting acidic and basic azoles in 1:3 or 1:1 stoichiometric compositions at elevated temperature, followed by saturation with  $Nd(OAc)_3$ · $xH_2O$  or  $Ce(OAc)_3$ · $xH_2O$ , which led to 13 new metal—acetate polymeric complexes identified by single-crystal X-ray diffraction. We found that the diversity in coordination modes of the simple acetate ligand that interfere with substitution of the softer N donors led to several readily crystallizable complexes forming two distinct groups with respect to f-element interaction with the ionic liquid precursors. When the acidic/basic azole ratio was 1:3, acetate and a neutral basic azole were found to be coordinated to the metal centers but no water, although in one case (2) water was observed in the secondary coordination sphere:



In water, annotagin in one case (2) water was observed in the secondary coordination sphere. [Ce( $\mu_2$ -OAc)<sub>3</sub>(C<sub>1</sub>im)]<sub>n</sub> (1, C<sub>1</sub>im = 1-methylimidazole), [Nd( $\mu_2$ -(OAc)<sub>3</sub>(C<sub>1</sub>im)]<sub>n</sub>·nH<sub>2</sub>O (2), [Ce( $\mu_2$ -OAc)<sub>3</sub>(C<sub>2</sub>im)]<sub>n</sub> (3, C<sub>2</sub>im = 1-ethylimidazole), [Ln( $\mu_2$ -OAc)<sub>3</sub>DMF]<sub>n</sub> (Ln = Nd (4), Ce (5); dimethylformamide (DMF) was substituted for the azole mixture), and [Nd( $\mu_2$ -OAc)<sub>3</sub>(C<sub>4</sub>im)]<sub>n</sub> (6, C<sub>4</sub>im = 1-butylimidazole). However, when the stoichiometric ratio was 1:1, water was always observed coordinated to the metal ions with the acidic azole included in the structure as a solvate or cocrystal, despite a higher reaction temperature: [Nd( $\mu_2$ -OAc)<sub>3</sub>(OH<sub>2</sub>)]<sub>n</sub>·n(1,2,3-Taz) (7, 1,2,3-Taz = 1,2,3-triazole), [Ln( $\mu_2$ -OAc)<sub>3</sub>(OH<sub>2</sub>)]<sub>n</sub>·n(4,5-DCim) (Ln = Nd (8), Ce (9), 4,5-DCim = 4,5-dicyanoimidazole), [Ln( $\mu_2$ -OAc)<sub>3</sub>(OH<sub>2</sub>)]<sub>n</sub>·n(3,5-diNH<sub>2</sub>-1,2,4-Taz) (Ln = Nd (10), Ce (11), 3,5-diNH<sub>2</sub>-1,2,4-Taz = 3,5-diamino-1,2,4-triazole), [Ce( $\mu_2$ -OAc)<sub>3</sub>(OH<sub>2</sub>)]<sub>n</sub>·n(3-NH<sub>2</sub>-1,2,4-Taz) (12, 3-NH<sub>2</sub>-1,2,4-Taz = 3-amino-1,2,4-triazole), and [Nd( $\mu_2$ -OAc)<sub>3</sub>(OH<sub>2</sub>)]<sub>n</sub>·n(5-NH<sub>2</sub>-Tz) (13, 5-NH<sub>2</sub>-Tz = 5-aminotetrazole). All of the compounds retain the Ln:OAc<sup>-</sup> ratio of 1:3 and form 1D polymeric chains; however, they exhibit a variety of coordination modes affecting the degree of chain condensation. The isolation of both hydrated and anhydrous products revealed different abilities of the investigated soft N-donors to compete with O-donors finding their place in the coordination sphere of the lanthanide or in the crystal lattice.

## **■ INTRODUCTION**

Separations of 4f from Sf elements is crucial in the recycling of spent nuclear fuel, 1-4 whose accumulation represents increasing hazards for the environment. These separations are often based on the slight preference of Sf elements for softer donors; 6,7 however, the issue of "covalency" if Sf complexes is still hotly debated 1 and f-orbital—ligand interactions represent significantly underexplored areas of chemical bonding. Such investigations are frequently hindered by the radioactive nature of the actinides, experimental difficulties due to the restricted amounts available, and strong competition with hard bases such as oxygen.

Application of ionic liquids (ILs) in the separation of lanthanides and actinides is promising but limited and still requires a fundamental understanding because the similar physicochemical properties of lanthanides and actinides complicate the process of separation. We have been investigating IL-based routes to develop a library of 5f soft donor complexes, which could be studied crystallographically

to help build better models for study. We have hypothesized that by dissolving f-element salts in ILs containing only soft donors (e.g., imidazoles) one could drive off volatiles, including water and carboxylic or mineral acids, leaving no choice but to complex the softer donors of the ILs.<sup>18</sup> We have previously shown that f-element salt hydrates can be dissolved and dehydrated in the ILs with a common anion (e.g., nitrate or acetate).<sup>19–21</sup>

Acetate-based ionic liquids not only serve as a reaction medium but also act as good dehydrating agents, allowing precise control over the course of the reaction.<sup>20</sup> The thermodynamic and electrochemical properties of the acetate-

Received: February 15, 2021 Revised: February 25, 2021 Published: March 16, 2021





Table 1. Experimental Details for the Preparation of Complexes 1-3 and 6

complex <sup>a</sup>	B-Az (3 equiv)	H-Az (1 equiv) 5-NH <sub>2</sub> -Tz (common)	metal salt	crystals within
$[Ce(\mu_2\text{-OAc})_3(C_1\text{im})]_n (1)$	C <sub>1</sub> im, 0.246 g (3 mmol)	0.085 g (1 mmol)	$Ce(OAc)_3 \cdot xH_2O$ (0.095 g)	60 days
$[\mathrm{Nd}(\mu_2\text{-}\mathrm{OAc})_3(\mathrm{C_1im})]_n \cdot n\mathrm{H}_2\mathrm{O} \ (2)$	C <sub>1</sub> im, 0.246 g (3 mmol)	0.085 g (1 mmol)	$Nd(OAc)_3 \cdot xH_2O(0.089 g)$	90 days
$[Ce(\mu_2\text{-OAc})_3(C_2\text{im})]_n$ (3)	C <sub>2</sub> im, 0.288 g (3 mmol)	0.085 g (1 mmol)	$Ce(OAc)_3 \cdot xH_2O$ (0.101 g)	68 days
$[\mathrm{Nd}(\mu_2\text{-}\mathrm{OAc})_3(\mathrm{C_4im})]_n$	$C_4$ im, 0.372 g (3 mmol)	0.085 g (1 mmol)	$Nd(OAc)_3 \cdot xH_2O$ (0.104 g)	80 days

<sup>&</sup>quot;An azole solution was first obtained by stirring the azole mixtures at 105 °C for 1 h. After metal salt saturation, the resulting reaction mixture was stirred at 105 °C for 2 h.

Table 2. Experimental Details for the Preparation of Complexes 7-13

1a	B-Az (1 equiv) 1-m-1,2,4-Taz	II A- (1i) (il)	metal salt	crystals within
complex <sup>a</sup>	(common)	H-Az (1 equiv) (varied)	metai sait	witnin
$[Nd(\mu_2-OAc)_3(OH_2)]_n \cdot n(1,2,3-Taz)$	0.083 g (1 mmol)	1,2,3-Taz, 0.069 g (1 mmol)	Nd(OAc)3 · xH2O      (0.091 g)	20 days
$[Nd(\mu_2-OAc)_2(OAc)(OH_2)_2]_n \cdot n(4,5-DCim)$ (8)	0.083 g (1 mmol)	4,5-DCim, 0.118 g (1 mmol)	Nd(OAc)3·xH2O (0.073 g)	5 days
$[Ce(\mu_2\text{-OAc})_2(OAc)(OH_2)_2]_n \cdot n(4,5\text{-DCim})$ (9)	0.083 g (1 mmol)	4,5-DCim, 0.118 g (1 mmol)	$Ce(OAc)_3 \cdot xH_2O$ $(0.081 g)$	7 days
$[Nd(\mu_2-OAc)_2(OAc)(OH_2)_2]_n \cdot n(3.5-diNH_2-1,2,4-Taz)$ (10)	0.083 g (1 mmol)	3,5-diNH <sub>2</sub> -1,2,4-Taz, 0.100 g (1 mmol)	$Nd(OAc)_3 \cdot xH_2O$ (0.078 g)	17 days
[Ce( $\mu_2$ -OAc) <sub>2</sub> (OAc)(OH <sub>2</sub> ) <sub>2</sub> ] <sub>n</sub> ·n(3,5-diNH <sub>2</sub> -1,2,4-Taz) (11)	0.083 g (1 mmol)	3,5-diNH <sub>2</sub> -1,2,4-Taz, 0.100 g (1 mmol)	$Ce(OAc)_3 \cdot xH_2O$ $(0.069 g)$	10 days
$[Ce(\mu_2\text{-OAc})_2(OAc)(OH_2)_2]_n \cdot n(3\text{-NH}_2\text{-}1,2,4\text{-Taz})$ (12)	0.083 g (1 mmol)	3-NH <sub>2</sub> -1,2,4-Taz, 0.084 g (1 mmol)	$Ce(OAc)_3 \cdot xH_2O$ $(0.082 g)$	15 days
$[\operatorname{Nd}(\mu_2\operatorname{-OAc})_2(\operatorname{OAc})(\operatorname{OH}_2)_2]_n \cdot n(\operatorname{S-NH}_2\operatorname{-Tz})$ (13)	0.083 g (1 mmol)	5-NH <sub>2</sub> -Tz, 0.085 g (1 mmol)	$Nd(OAc)_3 \cdot xH_2O$ (0.077 g)	9 days

<sup>&</sup>lt;sup>a</sup>The azole solution was obtained by stirring the azole mixtures at 120 °C for 1 h. The metal-saturated solutions were stirred at 120 °C for 2 h.

based ionic liquids have been actively investigated recently, particularly in light of  $\mathrm{CO}_2$  sorption.  $^{22-24}$  Our recent explorations revealed that particularly imidazolium-based acetate ILs showed perfect performance not only in dissolution of insoluble f-element oxides but also in dehydration of the formed complexes. However, while the formed acetate complexes show huge structural variability, they allow ready incorporation of soft N-donors, opening new experimental pathways and showing sensitivity to the cation size.

Because of the difficulty in using transuranic elements, we need to validate our methods first with 4f analogues and we need to find simple one-pot reactions to simplify the handling of the transuranic isotopes. We have chosen Nd³+ as an analogue for <sup>243</sup>Am³+ and Ce³+/Ce⁴+ as analogues for <sup>239</sup>Pu³+/Pu⁴+, given their charge to size ratios. Here we present our first results using this strategy. We found that the complexity of the simple acetate ligand leads to several readily crystallizable complexes that interfere with substitution of the softer N donors, forming two distinct groups with respect to f-element interactions with the ionic liquid precursors.

#### **■ EXPERIMENTAL SECTION**

**Materials.** Neodymium acetate hydrate,  $Nd(OAc)_3 \cdot xH_2O$ , cerium acetate hydrate,  $Ce(OAc)_3 \cdot xH_2O$ , 1-methylimidazole  $(C_1im)$ , 1-ethylimidazole  $(C_2im)$ , 1-butylimidazole  $(C_4im)$ , 5-aminotetrazole (5- $NH_2$ -Tz), 4,5-dicyanoimidazole (4,5-DCim), 3,5-diamino-1,2,4-triazole (3,5-di $NH_2$ -1,2,4-Taz), 3-amino-1,2,4-triazole (3- $NH_2$ -1,2,4-Taz), 1,2,3-triazole (1,2,3-Taz), 1-methyl-1,2,4-triazole (1-m-1,2,4-Taz), and methanol ( $CH_3OH$ ) were obtained from Sigma-Aldrich (St. Louis,  $CH_3OH$ ) was obtained from VWR International (Radnor,  $CH_3OH$ ) and used as received.

Crystallization of 1–3 and 6. In a representative experiment, 0.246 g (3 mmol) of  $C_1$ im and 0.085 g (1 mmol) of 5-NH<sub>2</sub>-Tz were

combined in a screw-top glass 2 dram (7.4 mL) vial. The vial was heated on a sand bath at 105 °C for 1 h to give a homogeneous azole mixture solution. To this was added  $Ce(OAc)_3 \cdot xH_2O$  portionwise slowly until saturation. The total amount of added metal salt was 0.095 g. The metal salt saturated azole solution was further heated for 2 h on a sand bath with constant stirring. After 2 h of heating a homogeneous solution was obtained. The solution was cooled slowly to RT by reducing the sand bath temperature 10 °C per step over a day. The resultant mixture was left undisturbed at RT for crystallization. Single-crystal X-ray diffraction (SCXRD) quality crystals of  $[Ce(\mu_2\text{-OAc})_3(C_1\text{im})]_n$  (1) were obtained over a period of 60 days. The reaction vial also contained crystals of S-NH<sub>2</sub>-Tz, as confirmed by SCXRD. Specific details for the other reactions are provided in Table 1.

Crystallization of [Ln( $\mu_2$ -OAc)<sub>3</sub>DMF]<sub>n</sub> (Ln = Nd (4), Ce (5)). A 0.050 mg portion of Ln(OAc)<sub>3</sub>:xH<sub>2</sub>O was suspended in 0.5 mL of DMF in a screw-top 2 dram glass vial and heated at reflux (153 °C) for 5 min for complete dissolution of the acetate salts. The clear solution was slowly cooled to RT, resulting in single crystals of good quality.

Crystallization of 7-13. In a representative experiment, 0.083 g (1 mmol) of 1-m-1,2,4-Taz and 0.118 g (1 mmol) of 4,5-DCim were placed in a screw-capped 2 dram glass vial. The reaction mixture was heated at 120 °C for 1 h with constant stirring until complete dissolution. The solution was then saturated with Nd(OAc)3·xH2O by portionwise addition. The added metal salt weight was found to be 0.073 g (0.23 mmol) at saturation. The saturated solution was further heated at 120 °C for 2 h. The reaction mixture was then slowly cooled to RT by reducing the sand bath temperature 10  $^{\circ}\text{C}$  per step. The reaction mixture solidified at RT. To obtain SCXRD-quality crystals, the resulting mass was layered with a 1/3 CH<sub>3</sub>OH/CH<sub>3</sub>CN solvent mixture to induce slow solvent diffusion crystallization. The undisturbed reaction vial at RT yielded SCXRD-quality crystals of  $[Nd(\mu_2-OAc)_2(OAc)(OH_2)_2]_n$ n(4,5-DCim) (8) after approximately 4-5 days. Specific details for the other related reactions are provided in Table 2.

Single-Crystal X-ray Diffraction (SCXRD). SCXRD data were measured on a Rigaku (Billerica, MA) diffractometer equipped with a fast  $\kappa$  geometry goniometer and hybrid pixel array (HyPix)

#### Scheme 1. Reaction Conditions

## (i) Synthesis of B-Az coordinated acetate complexes

# (ii) Synthesis of dihydrate acetate complexes

H-Az + 
$$N = 120$$
 °C, 1 h Azole solution  $+ Ln(OAc)_3 \cdot xH_2O$  Metal saturation  $+ Ln(OAc)_3 \cdot xH_2O$  [Ln( $\mu_2$ -(OAc) $\mu_2$ )]  $+ Ln(OAc)_3 \cdot xH_2O$ 

## (iii) Synthesis of DMF solvates

$$Ln(OAc)_3 \cdot xH_2O + DMF \xrightarrow{153 \circ C, 5 \text{ min}} [Ln(\mu_2 - (OAc)_3DMF]_n$$

Table 3. Basic Structural Parameters from the SCXRD Characterizations<sup>a</sup>

compound	a, Å	b, Å	c, Å	α, deg	$\beta$ , deg	γ, deg	<i>V</i> , Å <sup>3</sup>	space group
$[Ce(\mu_2\text{-OAc})_3(C_1\text{im})]_n$ (1)	18.0088(5)	8.4617(2)	18.4414(4)	90	90	90	2810.2(1)	Pbcn
$[Nd(\mu_2-(OAc)_3(C_1im)]_n-nH_2O$ (2)	18.4237(4)	8.3695(2)	18.4370(4)	90	90	90	2842.9(1)	Pbcn
$[Ce(\mu_2\text{-OAc})_3(C_2 \text{ m})]_n$ (3)	8.3564(1)	18.6780(3)	18.6963(3)	90	90	90	2918.13(7)	Pbca
$[Nd(\mu_2\text{-OAc})_3DMF]_n (4)$	9.3967(2)	17.1909(4)	8.3418(2)	90	93.734(2)	90	1344.66(5)	$P2_1/c$
$[Ce(\mu_2\text{-OAc})_3DMF]_n (5)$	9.4050(3)	17.2505(5)	8.4577(3)	90	93.562(3)	90	1369.53(8)	$P2_1/c$
$[Nd(\mu_2-OAc)_3(C_4 \text{ im})]_n$ (6)	7.8314(2)	16.0949(4)	13.6347(4)	90	105.345(3)	90	1657.33(8)	$P2_1/c$
$[Nd(\mu_2\text{-OAc})_3(OH_2)]_n \cdot n(1,2,3\text{-Taz})$ (7)	10.3422(3)	17.6605(4)	7.8044(2)	90	108.883(3)	90	1348.74(6)	$P2_1/c$
$[\operatorname{Nd}(\mu_2\operatorname{-OAc})_2(\operatorname{OAc})(\operatorname{OH}_2)]_n \cdot n(4,5-$ DCim) (8)	8.7114(1)	9.6218(1)	10.9072(1)	85.008(1)	70.586(1)	76.969(1)	839.98(2)	$P\overline{1}$
[Ce( $\mu_2$ -OAc) <sub>2</sub> (OAc) (OH <sub>2</sub> )] <sub>n</sub> ·n(4,5-DCim) (9)	8.7105(1)	9.6917(2)	10.8957(2)	84.973(2)	70.779(2)	77.137(2)	846.64(3)	$P\overline{1}$
$[Nd(\mu_2-OAc)_2(OAc) (OH_2)]_n \cdot n(3,5-diNH_2-1,2,4-Taz) (10)$	8.5037(1)	10.1683(1)	10.7862(1)	105.139(1)	108.603(1)	108.296(1)	768.62(2)	$P\overline{1}$
[Ce( $\mu_2$ -OAc) <sub>2</sub> (OAc) (OH <sub>2</sub> )] <sub>n</sub> ·n(3,5-diNH <sub>2</sub> -1,2,4-Taz) (11)	8.5133(1)	10.2036(1)	10.8668(1)	105.021(1)	108.711(1)	108.104(1)	779.37(2)	$P\overline{1}$
$[Ce(\mu_2\text{-OAc})_2(OAc)(OH_2)]_n \cdot n(3\text{-NH}_2-1,2,4\text{-Taz})$ (12)	8.6411(1)	9.3818(1)	11.0080(2)	113.573(1)	100.954(1)	104.009(1)	791.20(2)	$P\overline{1}$
$[Nd(\mu_2-OAc)_2(OAc)(OH_2)]_n \cdot n(5-NH_2-Tz)$ (13)	8.9353(1)	9.1205(1)	10.6320(2)	111.631(1)	102.977(1)	104.615(1)	729.18(2)	$P\overline{1}$

<sup>&</sup>quot;Abbreviations:  $C_1$  im = 1-methylimidazole,  $C_2$  im = 1-ethylimidazole,  $C_4$  im = 1-butylimidazole, DMF = dimethylformamide, 1,2,3-Taz = 1,2,3-triazole, 4,5-DCim = 4,5-dicyanoimidazole, 3,5-diNH<sub>2</sub>-1,2,4-Taz = 3,5-diamino-1,2,4-triazole, 3-NH<sub>2</sub>-1,2,4-Taz = 3-amino-1,2,4-triazole, 5-NH<sub>2</sub>-Tz = 5-aminotetrazole.

detector (XtaLAB Synergy R, DW) using Mo K $\alpha$  radiation (0.71073 Å). Crystals were mounted on a MiTeGen loop (MiTeGen LLC, Ithaca, NY) using Paratone (C) oil. The data collection was carried out at a steady temperature of -173 °C under a nitrogen gas stream using an Oxford Cryostreame 800 instrument. Data were collected using  $\omega$  scans with 0.5° frame width. The total number of runs and images was based on the strategy calculated from the program CrysAlisPro. Unit cell refinement, data reduction, scaling, and absorption correction were performed using CrysAlisPro. The structures were solved with the ShelXT<sup>27</sup> structure solution program using the intrinsic phasing solution method, applying Olex2<sup>28</sup> as the graphical interface. The model was refined by least squares using ShelXL.<sup>29</sup> All non-hydrogen atoms were refined anisotropically. Hydrogen atom positions were calculated geometrically and refined using the riding atom model. For the water molecules, hydrogen

atoms were refined with constrained O-H distances and with the nearest H-bond acceptors taken into account.

#### RESULTS AND DISCUSSION

**Synthetic Approaches.** Homoleptic anhydrous f-element complexes (e.g., acetates or nitrates) were found to be an affordable and preferred route for doing N-donor substitution in ILs and boiling off any water and other solvents. To obtain such complexes and further examine their ability to coordinate soft N donors *in situ*, we turned to protic ILs obtained by the reaction of an acidic and a basic azole. It was hoped that the presence of the acidic proton would facilitate combination with acetate to allow volatilization of HOAc.

Table 4. General Overview of the Newly Discovered and Related Ln-Acetate 1D Polymeric Acetates

Compound	Polymeric Structure <sup>a</sup>	Ln-Ln (Å)	Connectivity Side 1	Side 2	Non-bridging Ligands
1, 2, 3, 4, 5	*****	4.1781(2)-4.2481(3)	$2*\eta^3\mu_2\kappa^2+\eta^2\mu_2\kappa^2$	$2*\eta^3\mu_2\kappa^2+\eta^2\mu_2\kappa^2$	$C_1$ Im
6		4.0377(2) + 4.1955(3)	$2*\eta^3\mu_2\kappa^2+2*\eta^2\mu_2\kappa^2$	$2^*\eta^3\mu_2\kappa^2$	C <sub>4</sub> Im
7	***	4.1088(3)	$2*\eta^3\mu_2\kappa^2+\eta^2\mu_2\kappa^2$	$2*\eta^3\mu_2\kappa^2+\eta^2\mu_2\kappa^2$	H <sub>2</sub> O
8, 9, 10, 11, 12		4.3157(3)-4.6268(2)	$2*\eta^3\mu_2\kappa^2$	$2^*\eta^3\mu_2\kappa^2$	$\eta^2\mu\kappa^2 + 2H_2O$
13		4.2697(3) + 4.9831(3)	$2*\eta^3\mu_2\kappa^2$	$2*\eta^2\mu_2\kappa^2$	$\eta^2\mu\kappa^2 + 2H_2O$
$C_2 mim[Nd_2(OAc)_7]^{\underline{20}}$	X	4.1299(6) + 4.1949(6)	$2*\eta^3\mu_2\kappa^2+\eta^2\mu_2\kappa^2$	$2*\eta^3\mu_2\kappa^2+\eta^2\mu_2\kappa^2$	$0.5*\eta^2\mu\kappa^2$
$K_2Ce(OAc)_5 \cdot H_2O^{30}$	444	6.71(1)	$\eta^2 \mu_2 \kappa^2$	$\eta^2 \mu_2 \kappa^2$	$3*\eta^2\mu\kappa^2+\eta\mu\kappa$
RbLa(CH <sub>3</sub> COO) <sub>4</sub> <sup>31</sup> (b)		4.326(3) + 6.980(4)/6.980(4)	$2*\eta^3\mu_2\kappa^2$	$\eta^2 \mu_2 \kappa^2/\eta^2 \mu_2 \kappa^2$	
$Pr(OAc)_3 \cdot H_2O^{32}$	same as 7	4.217(1)	$2*\eta^3\mu_2\kappa^2+\eta^2\mu_2\kappa^2$	$2*\eta^3\mu_2\kappa^2+\eta^2\mu_2\kappa^2$	$H_2O$
$Nd(OAc)_3 \cdot 0.5 H_2 O^{33}$	A CANA	3.8970(5) + 4.1352(5)	$3*\eta^3\mu_2\kappa^2$	$2*\eta^3\mu_2\kappa^2+\eta^2\mu_2\kappa^2$	0.5*H <sub>2</sub> O
[Nd(OAc) <sub>3</sub> (HOAc)]·HOAc <sup>33</sup>	same as 6	4.0236(7) + 4.1884(9)	$2*\eta^{3}\mu_{2}\kappa^{2}+2*\eta^{2}\mu_{2}\kappa^{2}$	$2{*}\eta^3\mu_2\kappa^2$	ημκ
$[Nd(OAc)_3(HOAc)_2]\cdot HOAc^{\underline{33}}$	same as 8-12	4.4257(7) + 4.4469(7)	$2*\eta^3\mu_2\kappa^2$	$2*\eta^3\mu_2\kappa^2$	$\eta^2 \mu \kappa^2 + 2*\eta \mu \kappa$
Yb(OAc) <sub>3</sub> 33	***	4.203(2)	$\eta^3\mu_2\kappa^2+2*\eta^2\mu_2\kappa^2$	$\eta^3\mu_2\kappa^2+2*\eta^2\mu_2\kappa^2$	-

<sup>&</sup>quot;Acetate coordination modes are shown as  $\eta^3 \mu_2 \kappa^2$  in yellow,  $\eta^2 \mu_2 \kappa^2$  in green,  $\eta^2 \mu \kappa^2$  in violet, and  $\eta \mu \kappa$  in light blue.  $\eta$  represents the number of metal coordination bonds to a single ligand (please note that this deviates from IUPAC nomenclature, as the binding atoms are not contiguous),  $\mu$  specifies how many metal atoms are involved in binding with one ligand, and  $\kappa$  specifies how many atoms of a specific ligand bind to the metal atom. A schematic representation of the acetate modes is provided in Figure S3 in the Supporting Information.  ${}^b\text{RbLa}(\text{CH}_3\text{COO})_4$  is a 1D chain of dimers.

The initial reactions were carried out as noted in Scheme 1, where mixtures of acidic (H-Az) and basic (B-Az) azoles in 1:3 or 1:1 stochiometric ratios were formed first by heating. Then the resulting solutions or ILs were saturated with  $Nd(OAc)_3 \times H_2O$  or  $Ce(OAc)_3 \times H_2O$ . For comparison, we also report the results from simple dehydration of the lanthanide salts using DMF. Crystallization occurred after slow cooling at RT as a function of time in each group of complexes—after a couple of months for aprotic ILs (1–3, 6), several days for protic ILs (7–13), and instantly in the presence of DMF (4, 5).

Single-crystal X-ray diffraction (SCXRD) identified 13 new metal—acetate polymeric complexes (Table 3). When the H-Az:B-Az ratio was 1:3, acetate and a neutral basic azole were found to be coordinated to the metal centers but no water, although in one case (2) water was observed in the secondary coordination sphere. The DMF dehydration also led to an anhydrous compound with one DMF coordinated in a similar fashion to the basic azoles. However, when the

stoichiometry was 1:1, water was always observed coordinated to the metal ions with the acidic azole included in the structure as a solvate or cocrystal, despite the higher reaction temperature.

**Crystal Structures.** SCXRD analyses of the 13 isolated crystal structures revealed all 13 to be polymeric acetates of only 5 structural types with the differences primarily being in the different bridging modes of the coordinated acetate groups: 1–5, 6, 7, 8–12, and 13 (Table 4). All of the complexes show the prevalence of the two bridging modes  $\eta^3 \mu_2 \kappa^2$  and  $\eta^2 \mu_2 \kappa^2$ , though with different amounts and ratios. Most of the polymeric chains are quite symmetrical with respect to the propagating bridging modes except for 6 and 13. On the other hand, each Ln pair in the group 1–7 is bound on average by three acetate bridges, in contrast to two in 8–13. The latter also contain additional nonbridging acetate groups, while 7 is the only complex containing three acetate bridges and coordinated water.

Crystal Growth & Design pubs.acs.org/crystal Article

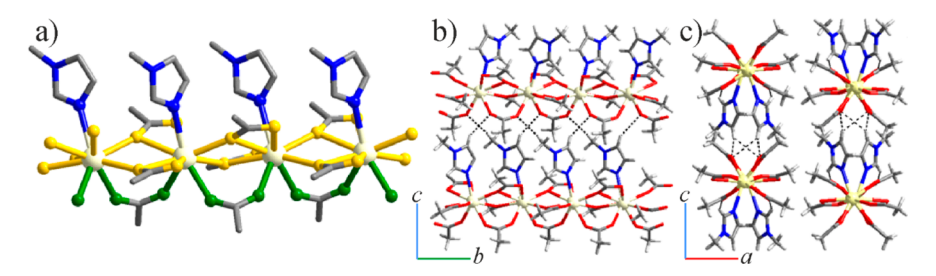


Figure 1. Bridging modes of acetates in  $1^*$  ( $\eta^3 \mu_2 \kappa^2$  and  $\eta^2 \mu_2 \kappa^2$  acetates in the 1D polymeric chain are represented in yellow and green, respectively) (a). Weak C-H···O hydrogen bonds holding the polymeric chains together to yield a 2D network structure in complex 1 (b). Projection of the 3D supramolecular network of 1 (c).  $1^*$  is considered as being representative of complexes 1–5.

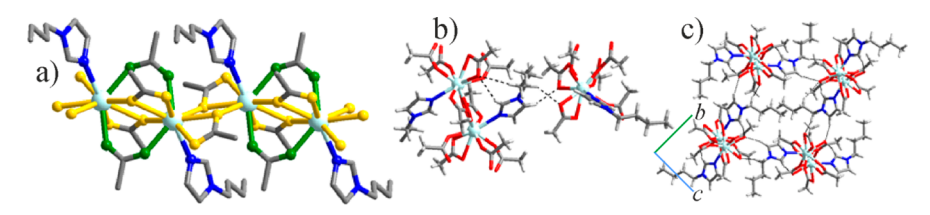


Figure 2. Coordination modes  $(\eta^3 \mu_2 \kappa^2)$  in yellow,  $\eta^2 \mu_2 \kappa^2$  in green) of acetate ions in the 1D polymeric chain of 6 (a). C–H···O hydrogen bonds between the imidazolium ring C–H and coordinated acetate (b). 3D supramolecular network of complex 6 (c).

 $Ce(\mu_2\text{-OAc})_3(C_1im)]_n$  (1),  $[Nd(\mu_2\text{-}(OAc)_3(C_1im)]_n\cdot nH_2O$  (2),  $[Ce(\mu_2\text{-OAc})_3(C_2im)]_n$  (3), and  $[Ln(\mu_2\text{-OAc})_3DMF]_n$  (Ln = Nd (4), Ce (5)). Complexes 1–5 are isostructural. with 1, 2 and 4, 5 being isomorphous pairs. 1 and 2 and 3 crystallize in the orthorhombic space groups *Pbcn* and *Pbca* (Z=8), respectively. 4 and 5 crystallize in the monoclinic space group  $P2_1/c$  (Z=4) and are isostructural with  $[Gd-(OAc)_3DMF]_n$ .

Each  ${\rm Ln}^{3+}$  cation is nine-coordinate connected to six bridging acetates and one N-donor (or DMF in 4 and 5) ligand (Figure 1). Of the three crystallographically independent acetate anions, two are in  $\eta^3\mu_2\kappa^2$  and one in  $\eta^2\mu_2\kappa^2$  bridging modes. The geometry around the  ${\rm Ln}^{3+}$  is a tricapped trigonal prism with two  $\eta^3\mu_2\kappa^2$  bidentate acetates occupying both capping vertexes and two bases, one  $\eta^3\mu_2\kappa^2$  bridging acetate occupying only a capping vertex. The remaining bases are occupied by one  $\eta^3\mu_2\kappa^2$  acetate, two  $\eta^2\mu_2\kappa^2$  acetates, and the N-donor/DMF ligand. The range of  ${\rm Ln-O}$  bond lengths for the  $\eta^3\mu_2\kappa^2$  acetates is 2.439(2)–2.650(2) Å, and that for  $\eta^2\mu_2\kappa^2$  acetates is 2.402(2)–2.455(3) Å. The  ${\rm Ln-N/Ln-O}$  (DMF) bond lengths range from 2.506(1) to 2.668(3) Å (Table S1 in the Supporting Information).

The adjacent metal centers are symmetrically bridged by three acetates; two are in the  $\eta^3\mu_2\kappa^2$  mode and one is in the  $\eta^2\mu_2\kappa^2$  mode to form an infinite polymeric chain (Figure 1a) along the a axis with an Ln···Ln separation range of 4.178(1)-4.248(1) Å. The dihedral angles between each pair of  $\eta^3\mu_2\kappa^2$  acetates and two  $\eta^2\mu_2\kappa^2$  acetates in the bridging link are  $\sim\!60$  and  $\sim\!68^\circ$ , respectively. N-donor/O-donor (DMF) ligands are attached to the metal—acetate polymeric chain as pendant groups and adopt a noncollinear arrangement with respect to each other to reduce steric hindrance (Figure 1a).

Intermolecular hydrogen-bonding interactions between hydrogen atoms of the imidazolium rings and  $\alpha$ -H of substituted alkyl chains of the ligands (N-donor,  $C_1$ im/ $C_2$ im; O-donor, DMF) and oxygen atoms of the coordinated carboxylate groups of the two adjacent chains form 2D networks in the bc plane (Figure 1b). These layers stick along

the *a* direction into a 3D network by means of van der Waals interactions (Figure 1c) or, in the case of **2**, are additionally enforced by indirect hydrogen bonding through the noncoordinated water molecules.

 $Nd(\mu_2\text{-}OAc)_3(C_4\text{im})]_n$  (6) and  $[Nd(\mu_2\text{-}OAc)_3(OH_2)]_n\cdot n(1,2,3\text{-}Taz)$  (7). Complexes 6 and 7 have structural features different from the rest of the group members and from each other, although they resemble 1–5 in terms of a single coordinated ligand ( $C_4\text{im}$  or water) to the 9-coordinated metal center other than bridging acetate ligands. 6 crystallizes in the monoclinic space group  $P2_1/c$  (Z=4). Similar to 1–5, out of the nine coordinating sites, eight are occupied by oxygen atoms from four  $\eta^3\mu_2\kappa^2$  and two  $\eta^2\mu_2\kappa^2$  acetates and the remaining site is occupied by the N-donor from  $C_4\text{im}$  (Figure 2).

The differences between 1–5 and 6 arise in the propagation mode of the polymeric chain. The four carboxylate groups from two  $\eta^3\mu_2\kappa^2$  acetates (shown in yellow) and two  $\eta^2\mu_2\kappa^2$  acetates (shown in green) coordinate two Nd³+ ions to form pseudo-paddlewheel-type dimers (Figure 2a). The consecutive dimers are further bridged by two  $\eta^3\mu_2\kappa^2$  acetates forming 1D polymeric chains (Figure 2a). This arrangement leads to unsymmetrical bridging between adjacent metal centers by two  $(\eta^3\mu_2\kappa^2)$  and four (two  $\eta^3\mu_2\kappa^2$ , two  $\eta^2\mu_2\kappa^2$ ) bridging acetates.

Dihedral angles between the planes of  $\eta^2 \mu_2 \kappa^2$  and  $\eta^3 \mu_2 \kappa^2$  acetates in the dimer with the  $\eta^3 \mu_2 \kappa^2$  acetate plane in the bridging link are 49.57 and 59.88°, respectively, with Nd···Nd distances of 4.0377(2) and 4.1955(3) Å, respectively.

The coordinated N-donor  $C_4$ im moieties on adjacent metal centers exhibit an anti orientation with respect to each other. Adjacent polymeric chains are oriented parallel to each other and are connected through intermolecular hydrogen-bonding interactions established between the imidazolium ring hydrogens,  $\alpha$ -H atoms of the substituted butyl chains, and oxygen atoms of the carboxylate groups in the bc plane, yielding a 3D supramolecular network (Figure 2b,c).

 $[Nd(\mu_2\text{-OAc})_3(OH_2)]_n \cdot n(1,2,3\text{-Taz})$  (7) possesses many common features with **6**, including the space group  $(P2_1/c, Z = 4)$ , coordination geometry (tricapped trigonal prism), and

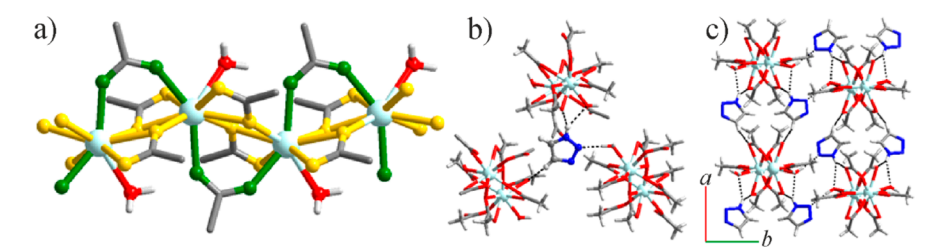
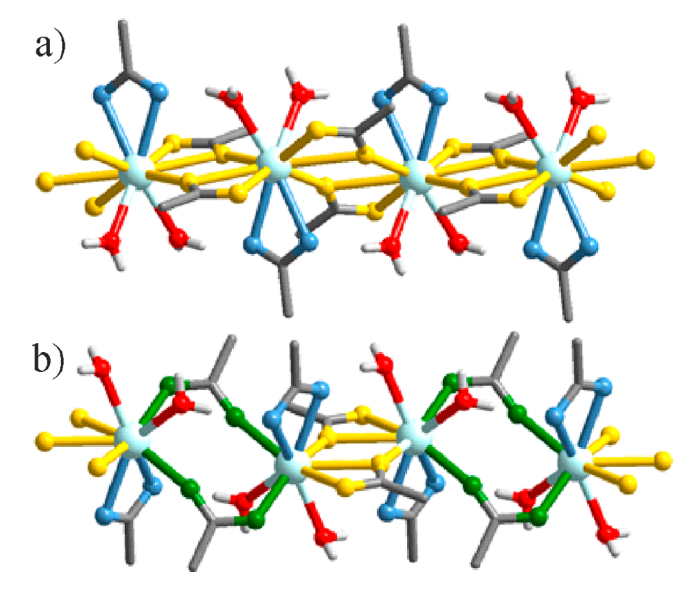


Figure 3. Acetate coordination modes  $(\eta^3 \mu_2 \kappa^2 \text{ in yellow}, \eta^2 \mu_2 \kappa^2 \text{ in green})$  in the 1D polymeric chain of 7 (a). Hydrogen bonding interactions of 1,2,3-Taz to monohydrate acetate polymeric chains (b). 3D supramolecular arrangement of 7 (c).

the acetate bridging modes (Figure 3a). However, unlike the asymmetric acetate bridging in 6, the acetate bridging in 7 is symmetrical as observed for 1-5, two  $\eta^3 \mu_2 \kappa^2$  and one  $\eta^2 \mu_2 \kappa^2$ acetate. The major difference arises in the orientation of the  $\eta^2 \mu_2 \kappa^2$  acetates with respect to each other. In 1–5, the dihedral angle between the  $\eta^2 \mu_2 \kappa^2$  acetates is approximately 68°, whereas in 7 the angle is 172°, leading to a sinusoidal arrangement in the polymeric chain (Figure 3a) instead of a pairwise arrangement as encountered in 1-5. This difference is further enhanced by the trans arrangement of the  $\eta^3 \mu_2 \kappa^2$ acetates and anti arrangement of the coordinated water molecules. The intrachain metal center separation distance is 4.1088(3) Å with Nd-O bond distances ranging from 2.444(1) to 2.546(2) Å for the  $\eta^{3}\mu_{2}\kappa^{2}$  acetates and 2.416(1)–2.479(1) Å for the  $\eta^{2}\mu_{2}\kappa^{2}$  acetates. Adjacent polymeric chains are held together by noncoordinated H-Az and 1,2,3-Taz through O-H···N and N-H···O hydrogen bonds (Figure 3b), resulting in a 3D supramolecular network (Figure 3c).

 $[Ln(\mu_2-OAc)_2(OAc)(OH_2)_2]_n\cdot n(4,5-DCim)$  (Ln = Nd (8), Ce (9)),  $[Ln(\mu_2 - OAc)_2(OAc)(OH_2)_2]_n \cdot n(3.5 - diNH_2 - 1.2.4 - Taz)$  (Ln = Nd (10), Ce (11)),  $[Ce(\mu_2-OAc)_2(OAc)(OH_2)_2]_n \cdot n(3-NH_2-1,2,4-1)$ Taz) (12), and  $[Nd(\mu_2-OAc)_2(OAc)(OH_2)_2]_n \cdot n(5-NH_2-Tz)$  (13). Complexes 8–13 crystallize in the triclinic space group  $P\overline{1}$  (Z = 2) with two coordinated water molecules and one noncoordinated H-Az in the crystal lattice. Complexes 8-12 have 10-coordinated Ln<sup>3+</sup> centers adopting a distortedbicapped-tetragonal antiprismatic geometry, whereas 13 has a 9-coordinated Nd<sup>3+</sup> center with a tricapped-trigonal-prismatic geometry. This difference arises due to the presence of different binding modes of the acetate anions. In the olymeric complexes 8-12, the acetates exhibit two types of binding modes,  $\eta^3 \mu_2 \kappa^2$  and  $\eta^2 \mu \kappa^2$  (Figure 4). The range of the Nd–O bond lengths for the  $\eta^3 \mu_2 \kappa^2$  acetate is 2.420(2)–2.873(2) Å and for the  $\eta^2 \mu \kappa^2$  acetate is 2.523(1)-2.573(2) Å (Table S1 in the Supporting Information).

On the other hand, the coordinated acetates in 13 exhibit  $\eta^3\mu_2\kappa^2$ ,  $\eta^2\mu\kappa^2$ , and  $\eta^2\mu_2\kappa^2$  binding modes with the Nd–O distances in the ranges 2.425(1)–2.647(1), 2.532(1)–2.588(1), and 2.388(1)–2.417(1) Å, respectively (Table S1 in the Supporting Information). These differences in the binding acetate modes and their ratio brings changes in the propagation pattern of the 1D polymeric chain. The adjacent metal centers in the polymeric chains of 8–12 are symmetrically bridged by two  $\eta^3\mu_2\kappa^2$  acetates (shown in yellow, Figure 4a), and the dihedral angle between each pair of  $\eta^3$ - $\mu_2$ - $\kappa^2$  acetates in this bridging link is ~40°. The bridging between the adjacent metal centers in the 1D polymeric chain of 13 is symmetrical with respect to the number of bridging acetates and unsymmetrical with respect to the coordination modes of the bridging acetates, including two



**Figure 4.** 1D polymeric chains encountered in complexes  $8^*$  (a), and 13 (b).  $8^*$  is considered as a representative for the group of complexes 8-12. Acetate coordination modes are shown as  $\eta^3 \mu_2 \kappa^2$  in yellow,  $\eta^2 \mu_2 \kappa^2$  in green, and  $\eta^2 \mu \kappa^2$  in light blue.

 $\eta^3\mu_2\kappa^2$  acetates (shown in yellow) and two  $\eta^2\mu_2\kappa^2$  acetates (shown in green) in an alternating fashion (Figure 4b). The dihedral angle between pairs of  $\eta^3\mu_2\kappa^2$  acetates and  $\eta^2\mu_2\kappa^2$  acetates in this bridging link is 37.82°. In both cases (8–12 and 13) a pair of water molecules and  $\eta^2\mu\kappa^2$  acetate (annotated blue) are trans with respect to each other.

In the supramolecular network, all of the dihydrate acetate complexes (8–13) exhibit a 3D hydrogen-bonded network built from 1D polymeric chains and noncoordinated lattice H-Az groups (Figure 5). Adjacent polymeric chains are held together through N–H···O and O–H···N hydrogen bonds, established between the noncoordinated acidic azoles and

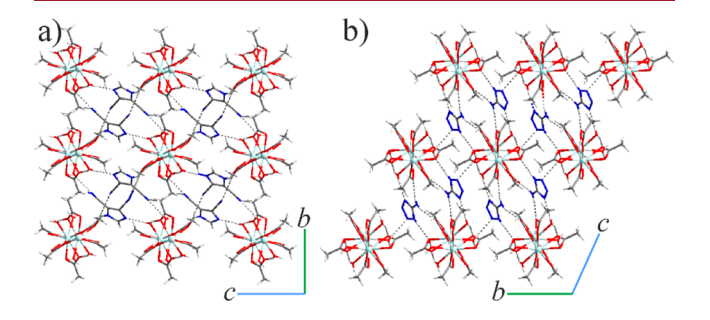
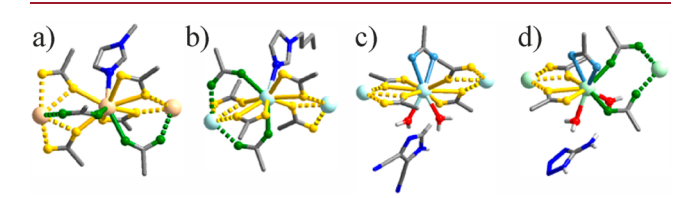


Figure 5. 3D supramolecular network with hydrogen-bonding interactions in 8 (a) and 13 (b).

coordinated [OAc]<sup>-</sup> anion and water molecules of the polymeric chains.

Analysis and Discussion. A geometrical analysis reveals that all of the acetate complexes with monocoordinated N-donor/O-donor (DMF/water, 1–7) and one of the dihydrated complexes (13) have nine-coordinated  ${\rm Ln}^{3+}$  centers with a distorted-tricapped-trigonal-prismatic geometry (Figure S1a in the Supporting Information). On the other hand, five of the dihydrated metal—acetate complexes (8–12) have 10-coordinated  ${\rm Ln}^{3+}$  with a distorted-bicapped-tetragonal-antiprismatic geometry (Figure S1a in the Supporting Information). The details on bond distances such as M–O/M–N and M–M are given in Table S1. In genera—l, while  ${\rm LnO}$  distances show good correlation with the acetate coordination mode,  ${\rm Ln-Ln}$  distances depend strongly mainly on the quantity and the type of the bridging acetate modes, with  $\eta^3\mu_2\kappa^2$  leading to denser packing.

In all of the complexes, the contribution of the acetate ligands to the coordination number is 8. The acetates in the coordination sphere display three types of binding modes: two bridging,  $\eta^3\mu_2\kappa^2$  (shown in yellow) and  $\eta^2\mu_2\kappa^2$  (shown in green), and one terminal,  $\eta^2\mu\kappa^2$  (shown in light blue), as shown in Figure 6. An  $\eta^3\mu_2\kappa^2$  acetate is observed in all 13



**Figure 6.** Distribution of  $[OAc]^-$  modes among intrachain  $Ln^{3+}$  centers in complexes 1-5 and 7 (a), complex 6 (b), complexes 8-12 (c), and complex 13 (d). The coordination modes observed in the complexes are shown in yellow  $(\eta^3\mu_2\kappa^2)$ , green  $(\eta^2\mu_2\kappa^2)$ , and light blue  $(\eta^2\mu\kappa^2)$ .

complexes, assisting in the formation of the polymeric chains. Terminal  $\eta^2 \mu \kappa^2$  acetates are exclusively encountered in the dihydrates, whereas bridging through  $\eta^2 \mu_2 \kappa^2$  is observed for all one N-donor/O-donor (DMF and H<sub>2</sub>O) coordinated acetate complexes and one dihydrate complex, 13. The CN 9 of this dihydrate, 13, is due to the presence of a  $\eta^2 \mu_2 \kappa^2$  bridging mode in a  $Z_i E$  conformation.

The formation of multiple binding modes of acetates can be attributed to the interplay between the charge compensation and the large coordination numbers in the felement complexes. Although  $\eta^3\mu_2\kappa^2$  bridging acetates assemble the polymeric chains, an  $\eta^2\mu_2\kappa^2$  bridging acetate has a unique arrangement in the complexes, which leads to the diversity in the coordination sphere arrangements. For instance, in complexes 1–5 and 7, the adjacent metal centers are symmetrically bridged by three acetates, two in the  $\eta^3\mu_2\kappa^2$  mode and one in the  $\eta^2\mu_2\kappa^2$  mode on each side (Figure 6a). In complex 6, four acetates, two each of the  $\eta^3\mu_2\kappa^2$  and  $\eta^2\mu_2\kappa^2$  modes, bridge on one side and only two  $\eta^3\mu_2\kappa^2$  acetates bridge on the other side of the metal centers (Figure 6b).

For complexes 8–12 the bridging between adjacent Ln<sup>3+</sup> centers is symmetrical through two  $\eta^3 \mu_2 \kappa^2$  acetates (Figure 6c). Nd<sup>3+</sup> centers in 13 are bridged unsymmetrically by two  $\eta^3 \mu_2 \kappa^2$  and two  $\eta^2 \mu_2 \kappa^2$  acetates in an alternating fashion (Figure 6d). This feature of acetates leads to similar

structures for 1-5, as shown in the overlay diagram (Figure 7), and for the dihydrated acetate complexes 8-13 (Figure

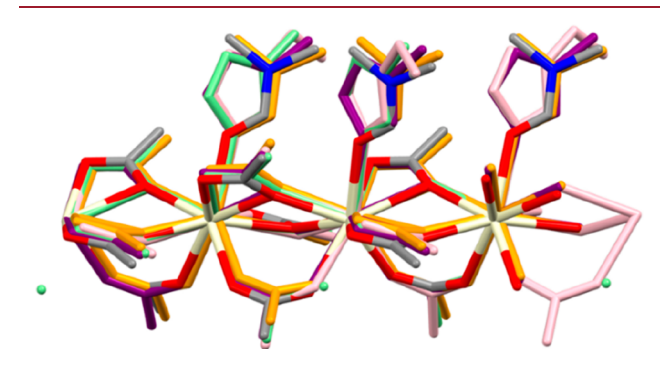


Figure 7. Overlay of 1D polymeric chains of the complexes 1 (purple), 2 (light green), 3 (pink), 4 (orange), and 5 (by element colors). Hydrogens are not shown for clarity.

8). The slight changes in acetate bridging fashion in 13 do not induce any structural distinguishability from the rest of the dihydrate complexes 8-12.

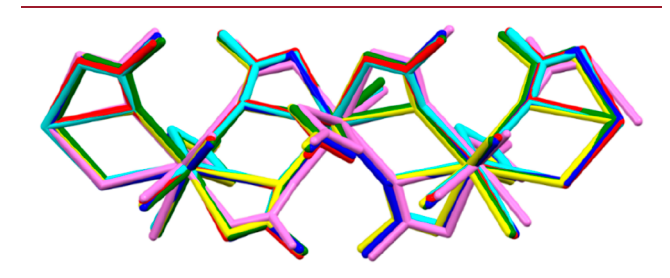


Figure 8. Overlay of 1D polymeric chains of complexes 8 (cyan), 9 (red), 10 (yellow), 11 (green), 12 (blue), and 13 (violet). Hydrogens are not shown for clarity.

A general overview of the coordination modes in various 1D polymeric lanthanide acetates is provided in Table 4. Nd complexes 2 and 8 have been chosen as the representatives for their corresponding series of relatives 1–5 and 8–12, respectively. Among these, RbLa(CH<sub>3</sub>COO)<sub>4</sub><sup>30–32</sup> has a single exclusion and represents a double polymeric chain or a chain based on nine-coordinated La dimers bridged by two acetates in  $\eta^3\mu_2\kappa^2$  mode. With respect to composition, most of the compounds exhibit a 3:1 OAc<sup>-</sup>:Ln ratio, which appears to be a magic number or necessary condition for the formation of a polymeric chain. However, larger light lanthanides such as Ce and Nd have extra space in their coordination spheres in comparison to heavy lanthanides and, if there are no additional nonbridging ligands, offer formation of more complex 2D or 3D frameworks, as observed in the anhydrous  $\text{Ln}(\text{OAc})_3^{35}$  (Ln = La, Pr, Nd) vs anhydrous  $\text{Yb}(\text{OAc})_3^{33}$  or in the dicyanamide series from La to Yb.  $^{36}$ 

In 1–7 the polymeric chains are rather compact, which is characterized by two factors, the total number of bridging acetates and the high proportion of the  $\eta^3\mu_2\kappa^2$  mode, affecting Ln–Ln intrachain distances. In this respect 1–5 and 7 have strong analogies with the recently discovered series  $[C_2\text{mim}][\text{Ln}_2(\text{OAc})_7]^{.20}$  The latter formally deviates from the 3:1 OAc<sup>-</sup>:Ln ratio, but one of the acetate groups is nonbridging, in fact substituting for the respective position of the N-/O-donor in 1–5. The same situation is in fact observed in two Nd acetate solvates,  $[\text{Nd}(\text{OAc})_3(\text{HOAc})]$ .

Crystal Growth & Design pubs.acs.org/crystal Article

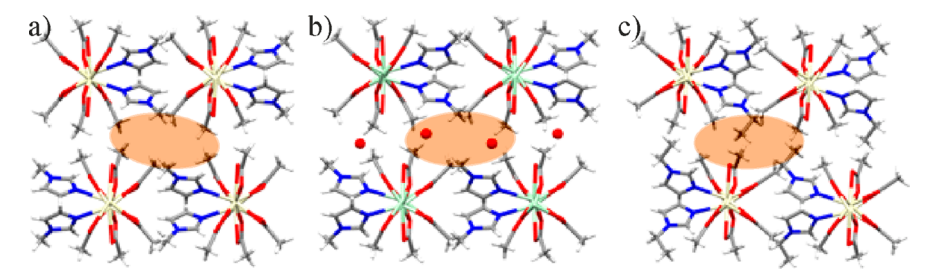


Figure 9. Depiction of the cavity in complex 1 (a) occupied by water molecules in complex 2 (b) and the  $\beta$  carbon of the ethyl group in complex 3 (c).

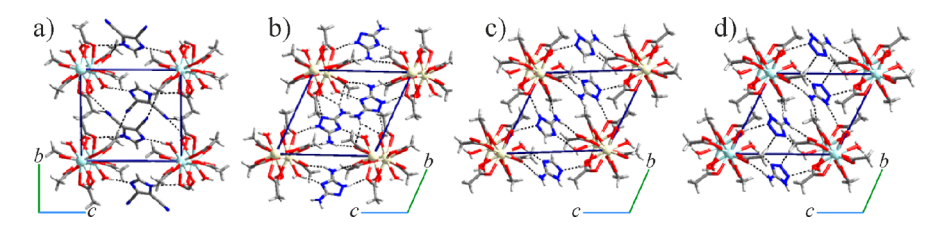


Figure 10. Unit cell packing of complexes 8 (a), 11 (b), 12 (c), and 13 (d) along the a axis.

HOAc and  $[Nd(OAc)_3(HOAc)_2]$ ·HOAc, where acetic acid is only occupying space in the coordination sphere of the lanthanide. We also do not count here double salts with alkali-metal cations, as they affect the total charge balance with respect to the stoichiometry.

The situation in 8–13 is somewhat different—the lower amount of bridging modes is compensated by terminal acetates and coordinated water, leading to a significant increase in the Ln–Ln distances. The quality and quantity of the nonbridging ligands does not play any significant role and is rather a consequence of intrachain connectivity. The extreme case is represented by the double salt RbLa- $(CH_3COO)_4$ , where single  $\eta^2\mu_2\kappa^2$  bridges lead to an enormous elongation of the Ln–Ln separations of up to  $\sim$ 7 Å.

The unit cell parameters shown in Table 1 also supports the above facts of structural similarity among the acetate complexes 1–5 and 8–13 separately. It is interesting to note that complexes 1–3 show close unit cell parameters in spite of the fact that 2 has an extra lattice water and 3 has ethyl substitution in the coordinated base in comparison to methyl substitution in 1. In this regard the structural packings of 1–3 along a crystallographic direction as shown in Figure 9 is interesting, because a small cavity generated in complex 1 is being occupied by water in 2 and by the second carbon of the ethyl group in 3.

The structural correlation of complexes 4 and 5 with 1 might be due to the similar dimensions and geometries of DMF and  $C_1$ im units, as shown in Figure S2 in the Supporting Information. While 8, 9 and 10, 11 are isomorphous pairs and there is a similarity in polymeric chains of 8–13, the variation in the geometry of the H-Az brings minor diversity into their packing. The unique structures 8 and 11–13 are compared in Figure 10. While the metal centers in 8 are in a rectangular arrangement, the others show a parallelogram arrangement that might be due to the entirely different geometry of 4,5-DCim comparison to the other amino azoles. Within the amino H-Az complexes, the unit cell length along the c axis is highest for 3,5-diNH<sub>2</sub>-1,2,4-Taz (11) due to the extra amino group in comparison to 3-NH<sub>2</sub>-1,2,4-Taz (12) and 5-NH<sub>2</sub>-Tz (13). Between 12

and 13, 5-NH<sub>2</sub>-Tz (13) has a shorter length along the c axis in comparison to 3-NH<sub>2</sub>-1,2,4-Taz (12). The possible reason for the shorter length in 13 may be the C-H···O hydrogen bond between the N3 nitrogen of the azole and the methyl group of the acetate. In a similar position, the carbon in 3-NH<sub>2</sub>-1,2,4-Taz with the hydrogen poses steric hindrance, leading to a longer distance. For the same C-H···O hydrogen bonds, the unit cell b parameter is shorter for 13 in comparison to the other three structures.

## SUMMARY

We have reported here the synthesis and crystal structures of a series of polymeric lanthanide acetates with various N-/Odonors. The entire series can formally be distributed into two principally different subgroups on the basis of the ability of the IL precursors to coordinate to the lanthanide ion and compete with hard O-donors. The first group includes alkylimidazole moieties that were able to coordinate directly to the lanthanides and to eliminate water from the coordination sphere. The use of DMF for the dehydration was also successful. The second group includes the acidic azoles 4,5-DCim, 1,2,3-Taz, 3-NH<sub>2</sub>-1,2,4-Taz, 3,5-diNH<sub>2</sub>-1,2,4-Taz, and 5-NH<sub>2</sub>-Tz, which were not able to compete with the coordinated water but remained in the system through hydrogen-bonding interactions.

The use of various secondary ligands did not affect the stoichiometry of counterions in the final products (Ln:OAcratio 3:1) or the connectivity modes, though they did affect their relative contributions. All of the complexes form 1D chains with a major involvement of the two bridging acetate modes  $\eta^3 \mu_2 \kappa^2$  and  $\eta^2 \mu_2 \kappa^2$ , with each pair of Ln atoms in the chain being bound by two or three acetate anions. Such a connectivity leads to fairly condensed packing with intrachain Ln-Ln distances varying in the range ~4.0-4.5 Å. These distances strongly correlate with the number of the bridging ligands, with 1- occupying the lower side of the range and 8-13 the upper side, following the tendency of related polymeric acetates from the literature. Nonbridging acetate groups and secondary ligands were found to contribute insignificantly to the chain density. The polymeric chains stack via direct aromatic C-H···O hydrogen bonds or van

der Waals interactions between the acetate  $CH_3$  groups. The density of hydrogen-bonding interactions in 8-13, however, is significantly enhanced due to coordinated water molecules and interstitial N-donors with multiple H-donors and acceptors.

The most significant synthetic finding was that a higher ratio of the basic azole in relation to the acidic azole was needed to force N-donor coordination. An acidic to basic azole stoichiometry of 1:3 led to exclusion of water from the metal coordination sphere (1-3, 6) and, except for 2, exclusion of water completely. However, when the stoichiometry was 1:1 (7-13), water was always found in the metal ion's inner coordination sphere and the azole hydrogen bonded in the outer coordination sphere, even when a higher reaction temperature was used. Overall, this suggests that our original strategy to simply dehydrate and force N-donor coordination by dissolving hydrated f-element salts in, essentially, a "sea of N donors", as in an IL environment, will ultimately be fruitful.

## ASSOCIATED CONTENT

## Supporting Information

The Supporting Information is available free of charge at https://pubs.acs.org/doi/10.1021/acs.cgd.1c00181.

Figures and a table as described in the text (PDF)

#### **Accession Codes**

CCDC 2053406-2053418 contain the supplementary crystallographic data for this paper. These data can be obtained free of charge via <a href="www.ccdc.cam.ac.uk/data\_request/cif">www.ccdc.cam.ac.uk/data\_request/cif</a>, or by emailing data\_request@ccdc.cam.ac.uk, or by contacting The Cambridge Crystallographic Data Centre, 12 Union Road, Cambridge CB2 1EZ, UK; fax: +44 1223 336033.

## **■** AUTHOR INFORMATION

## **Corresponding Authors**

Anja-Verena Mudring — Department of Materials and Environmental Chemistry, Stockholm University, Stockholm 10691, Sweden; orcid.org/0000-0002-2800-1684; Email: anja-verena.mudring@mmk.su.se

Robin D. Rogers — College of Arts & Sciences, The University of Alabama, Tuscaloosa, Alabama 35487, United States; Department of Materials and Environmental Chemistry, Stockholm University, Stockholm 10691, Sweden; orcid.org/0000-0001-9843-7494; Email: rdrogers@ua.edu

#### **Authors**

Amrita Nayak — College of Arts & Sciences, The University of Alabama, Tuscaloosa, Alabama 35487, United States Volodymyr Smetana — Department of Materials and Environmental Chemistry, Stockholm University, Stockholm 10691, Sweden; orcid.org/0000-0003-0763-1457

Complete contact information is available at: https://pubs.acs.org/10.1021/acs.cgd.1c00181

#### **Notes**

The authors declare no competing financial interest.

## ACKNOWLEDGMENTS

This research was supported, in part, by the Royal Swedish Academy of Science through the Göran Gustafsson prize to A.-V.M., by the Swedish Research Council (Vetenskapsrådet, VR) through Grant 2020-05405 (A.-V.M.), by a Tage Erlander Guest Professorship to R.D.R. (VR Grant 2018-00233), and by the U.S. Department of Energy, Office of Science, Office of Basic Energy Sciences, Heavy Elements program, under Award DE-SC0019220 (to R.D.R.). The SCXRD instrumentation at UA was supported by U.S. NSF MRI 1828078.

# **■** REFERENCES

- (1) Billard, I.; Ouadi, A.; Gaillard, C. Liquid-liquid extraction of actinides, lanthanides, and fission products by use of ionic liquids: from discovery to understanding. *Anal. Bioanal. Chem.* **2011**, 400, 1555–1566.
- (2) Takao, K.; Bell, T. J.; Ikeda, Y. Actinide chemistry in ionic liquids. *Inorg. Chem.* **2013**, *52*, 3459–3472.
- (3) Macerata, E.; Mossini, E.; Scaravaggi, S.; Mariani, M.; Mele, A.; Panzeri, W.; Boubals, N.; Berthon, L.; Charbonnel, M.-C.; Sansone, F.; Arduini, A.; Casnati, A. Hydrophilic Clicked 2,6-Bis-triazolyl-pyridines Endowed with High Actinide Selectivity and Radiochemical Stability: Toward a Closed Nuclear Fuel Cycle. *J. Am. Chem. Soc.* 2016, 138, 7232–7235.
- (4) Yin, X.; Wang, Y.; Li, X.; Xie, J.; Silver, M. A.; Chen, L.; Sheng, D.; Ji, G.; Chai, Z.; Wang, S. Competing Crystallization between Lanthanide and Actinide in Acidic Solution Leading to Their Efficient Separation. *Chin. J. Chem.* **2019**, *37*, 53–57.
- (5) Johnson, J. Decades for Decommissioning *Chem. Eng. News* 2014, 92, 22–23; https://cen.acs.org/articles/92/i22/Decades-Decommissioning.html
- (6) Hudson, M. J.; Harwood, L. M.; Laventine, D. M.; Lewis, F. W. Use of Soft Heterocyclic N-Donor Ligands To Separate Actinides and Lanthanides. *Inorg. Chem.* **2013**, *52*, 3414–3428.
- (7) Lewis, F. W.; Harwood, L. M.; Hudson, M. J.; Drew, M. G. B.; Desreux, J. F.; Vidick, G.; Bouslimani, N.; Modolo, G.; Wilden, A.; Sypula, M.; Vu, T.-H.; Simonin, J.-P. Highly Efficient Separation of Actinides from Lanthanides by a Phenanthroline-Derived Bis-triazine Ligand. *J. Am. Chem. Soc.* **2011**, *133*, 13093–13102.
- (8) Nash, K. L. Separation chemistry for lanthanides and trivalent actinides. In *Handbook on the physics and chemistry of rare earths*; Gschneidner, K. A., Eyring, L., Choppin, G. R., Lander, G. H., Eds.; Elsevier Science: Amsterdam, 1994; Vol. 18, pp 197–238.
- (9) Neidig, M. L.; Clark, D. L.; Martin, R. L. Covalency in f-element complexes. *Coord. Chem. Rev.* **2013**, 257, 394–406.
- (10) Kerridge, A. Quantification of f-element covalency through analysis of the electron density: insights from simulation. *Chem. Commun.* **2017**, 53, 6685–6695.
- (11) Lu, E.; Sajjad, S.; Berryman, V. E. J.; Wooles, A. J.; Kaltsoyannis, N.; Liddle, S. T. Emergence of the structure-directing role of f-orbital overlap-driven covalency. *Nat. Commun.* **2019**, *10*, 634.
- (12) Lukens, W. W.; Speldrich, M.; Yang, P.; Duignan, T. J.; Autschbach, J.; Kögerler, P. The roles of 4f- and 5f-orbitals in bonding: a magnetochemical, crystal field, density functional theory, and multi-reference wavefunction study. *Dalton Trans.* **2016**, *45*, 11508–11521.
- (13) Zbiri, M.; Daul, C. A.; Wesolowski, T. A. Effect of the f-Orbital Delocalization on the Ligand-Field Splitting Energies in Lanthanide-Containing Elpasolites. J. Chem. Theory Comput. 2006, 2, 1106–1111.
- (14) Billard, I.: Ionic Liquids: New Hopes for Efficient Lanthanide/Actinide Extraction and Separation? In *Handbook on the Physics and Chemistry of Rare Earths*; Bünzli, J.-C. G., Pecharsky, V. K., Eds.; Elsevier: 2013; Vol. 43; Chapter 256, pp 213–273.
- (15) Shkrob, I. A.; Marin, T. W.; Jensen, M. P. Ionic Liquid Based Separations of Trivalent Lanthanide and Actinide Ions. *Ind. Eng. Chem. Res.* **2014**, *53*, 3641–3653.
- (16) Berton, P.; Kelley, S. P.; Rogers, R. D. Ionic liquids for sustainable production of actinides and lanthanides, In *Metal*

- Sustainability: Global Challenges, Consequences, and Prospects; Izatt, R. M., Ed.; Wiley: Chichester, U.K., 2016; pp 295-316.
- (17) Straka, M. Toward a Greenish Nuclear Fuel Cycle: Ionic Liquids as Solvents for Spent Nuclear Fuel Reprocessing and Other Decontamination Processes for Contaminated Metal Waste. *Physical Sciences Reviews* **2016**, *1*, 20160074.
- (18) Kelley, S. P.; Smetana, V.; Emerson, S. D.; Mudring, A.-V.; Rogers, R. D. Benchtop access to anhydrous actinide N-donor coordination complexes using ionic liquids. *Chem. Commun.* **2020**, *56*, 4232–4235.
- (19) Kelley, S. P.; Smetana, V.; Nuss, J. S.; Dixon, D. A.; Vasiliu, M.; Mudring, A.-V.; Rogers, R. D. Dehydration of UO<sub>2</sub>Cl<sub>2</sub>·3H<sub>2</sub>O and Nd(NO<sub>3</sub>)<sub>3</sub>·6H<sub>2</sub>O with a Soft Donor Ligand and Comparison of Their Interactions through X-ray Diffraction and Theoretical Investigation. *Inorg. Chem.* **2020**, *59*, 2861–2869.
- (20) Bousrez, G.; Renier, O.; Kelley, S. P.; Adranno, B.; Tahavori, E.; Titi, H. M.; Smetana, V.; Tang, S.-F.; Mudring, A.-V.; Rogers, R. D. Ready access to anhydrous anionic lanthanide acetates using imidazolium acetate ionic liquids as the reaction medium. *Chem. Eur. J.*, accepted, **2021**.
- (21) Smetana, V.; Kelley, S. P.; Titi, H. M.; Hou, X.; Tang, S.-F.; Mudring, A.-V.; Rogers, R. D. Synthesis of Anhydrous Acetates for the Components of Nuclear Fuel Recycling in Dialkylimidazolium Acetate Ionic Liquids. *Inorg. Chem.* **2020**, *59*, 818–828.
- (22) Lepre, L. F.; Szala-Bilnik, J.; Padua, A. A. H.; Traïkia, M.; Ando, R. A.; Costa Gomes, M. F. Tailoring the properties of acetate-based ionic liquids using the tricyanomethanide anion. *Phys. Chem. Chem. Phys.* **2016**, *18*, 23285–23295.
- (23) Kasprzak, D.; Stępniak, I.; Galiński, M. Acetate- and lactate-based ionic liquids: Synthesis, characterisation and electrochemical properties. *J. Mol. Liq.* **2018**, *264*, 233–241.
- (24) Almeida, H. F. D.; Passos, H.; Lopes-Da-Silva, J. A.; Fernandes, A. M.; Freire, M. G.; Coutinho, J. A. P. Thermophysical Properties of Five Acetate-Based Ionic Liquids. *J. Chem. Eng. Data* **2012**, *57*, 3005–3013.
- (25) Cosier, J.; Glazer, A. M. A nitrogen-gas-stream cryostat for general X-ray diffraction studies. *J. Appl. Crystallogr.* **1986**, *19*, 105–107.
- (26) CrysAlisPRO; Oxford Diffraction/Agilent Technologies UK Ltd.: Yarnton, England.
- (27) Sheldrick, G. SHELXT Integrated space-group and crystal-structure determination. *Acta Crystallogr., Sect. A: Found. Adv.* **2015**, 71, 3–8.
- (28) Dolomanov, O. V.; Bourhis, L. J.; Gildea, R. J.; Howard, J. A. K.; Puschmann, H. OLEX2: a complete structure solution, refinement and analysis program. *J. Appl. Crystallogr.* **2009**, 42, 339–341.
- (29) Sheldrick, G. Crystal structure refinement with SHELXL. *Acta Crystallogr., Sect. C: Struct. Chem.* **2015**, 71, 3–8.
- (30) Sadikov, G. G.; Kukina, G. A.; Porai-Koshits, M. A.; Pospelova, L. A. X-ray structure of dipotassium cerium pentaacetate monohydrate. *J. Struct. Chem.* **1968**, *9*, 145.
- (31) Meyer, G.; Kutlu, I. Synthesis and Crystal Structure of Rubidium Lanthanum Tetraacetate, RbLa(CH<sub>3</sub>COO)<sub>4</sub>. Z. Anorg. Allg. Chem. **2000**, 626, 975–977.
- (32) Ganapathy, S.; Chacko, V. P.; Bryant, R. G.; Etter, M. C. Carbon CP-mass NMR and x-ray crystal structure of paramagnetic lanthanide acetates. *J. Am. Chem. Soc.* **1986**, *108*, 3159–3165.
- (33) Gomez, S. T. Thesis, Köln, Germany, 2007.
- (34) Roubeau, O.; Lorusso, G.; Teat, S. J.; Evangelisti, M. Cryogenic magneto-caloric effect and magneto-structural correlations in carboxylate-bridged Gd(iii) compounds. *Dalton Trans.* **2014**, *43*, 11502–11509.
- (35) Gomez Torres, S.; Meyer, G. Anhydrous Neodymium(III) Acetate. Z. Anorg. Allg. Chem. 2008, 634, 231–233.
- (36) Tang, S.-F.; Smetana, V.; Mishra, M. K.; Kelley, S. P.; Renier, O.; Rogers, R. D.; Mudring, A.-V. Forcing Dicyanamide Coordination to f-Elements by Dissolution in Dicyanamide-Based Ionic Liquids. *Inorg. Chem.* **2020**, *59*, 7227–7237.